

Masked Pre-trained Model Enables Universal Zero-shot Denoiser

Xiaoxiao Ma^{1*} Zhixiang Wei^{1*} Yi Jin^{1*} Pengyang Ling^{1,2} Tianle Liu¹ Ben Wang¹ Junkang Dai¹
Huaian Chen^{1†} Enhong Chen¹

¹ University of Science and Technology of China ² Shanghai AI Laboratory

{xiao.xiao,zhixiangwei,lpyang27,tleliu,wblzgrsn,junkangdai,anchen}@mail.ustc.edu.cn
{jinyi08,cheneh}@ustc.edu.cn

Abstract

In this work, we observe that the model, which is trained on vast general images using masking strategy, has been naturally embedded with the distribution knowledge regarding natural images, and thus spontaneously attains the underlying potential for strong image denoising. Based on this observation, we propose a novel zero-shot denoising paradigm, i.e., **Masked Pre-train then Iterative fill (MPI)**. MPI pre-trains a model with masking and fine-tunes it for denoising of a single image with unseen noise degradation. Concretely, the proposed MPI comprises two key procedures: 1) Masked Pre-training involves training a model on multiple natural images with random masks to gather generalizable representations, allowing for practical applications in varying noise degradation and even in distinct image types. 2) Iterative filling is devised to efficiently fuse pre-trained knowledge for denoising. Similar to but distinct from pre-training, random masking is retained to bridge the gap, but only the predicted parts covered by masks are assembled for efficiency, which enables high-quality denoising within a limited number of iterations. Comprehensive experiments across various noisy scenarios underscore the notable advances of proposed MPI over previous approaches with a marked reduction in inference time. Code is available at <https://github.com/krennic999/MPI.git>.

1. Introduction

Image denoising [8, 28], as a branch of image restoration, has been the subject of extensive exploration. The prevalent approach to restore noise-degraded images is learning from multiple noisy instances. Nonetheless, both supervised learning from noisy-clean pairs [24, 51, 52] and unsupervised training [12, 16, 22] necessitate the collection of additional noisy datasets. Moreover, such methods may

*Equal contribution.

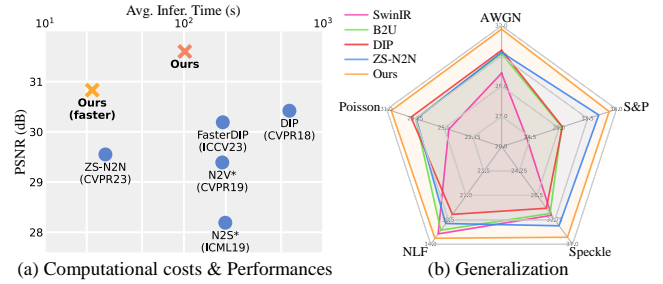


Figure 1. Comparison of computational costs, performances & generalization capability. (a) Our paradigm surpasses current zero-shot methods with reduced inference time (on CSet with AWGN $\sigma=25$, see Sec. 4.2). (b) It shows greater adaptability and generalization across different noise types compared to current zero-shot and supervised/unsupervised methods (See Sec. 4.3).

foster dependencies on patterns of training noise, hindering their performance in unfamiliar noise situations [5, 6].

As an alternative, zero-shot approaches [7, 39, 41] attempt to infer a corresponding clean image from a single noisy counterpart, thus negating the need for additional noisy data collection. Dedicated to obviating concerns about generalization issues, these techniques include blind-spot networks that reconstruct from corrupted inputs [4, 19], DIPs [15, 18, 27, 40, 41] which exploit the characteristics of deep networks to learn the mapping from random noise to noisy images, as well as sub-sample based strategies [23, 30] utilize spatial correlations to generate training pairs from sub-sampled instances.

However, due to the ill-posed nature [10, 48] of denoising, the reliance on crafted priors becomes necessary, which in turn reduces their robustness to different noisy scenarios. For instance, DIPs might produce images with incomplete noise removal or excessively blurry images due to their reliance on frequency-domain properties of deep models. Some methods [8, 18, 29] are specific to certain noise types and rely on known noise intensity. While sub-sample [23, 30] and blind-spot [4, 19] based strategies, relying on large mask proportions or strong sub-sampling on a single image, pose challenges in simultaneously removing

noise and reconstructing image details. Additionally, the high computational demands of current zero-shot methods also restrict their practical application.

Compared to priors utilized in previous works, learning the feature distribution from a vast amount of natural images offers a more intuitive approach. This is grounded in two considerations: 1) Real natural images are both abundant and readily available. 2) Regardless of variations in noise patterns, many natural images exhibit common characteristics [33]. To learn the latent distribution of natural images, we explore the potential of self-supervised learning [14, 46] on a large image dataset with no assumptions about noisy types and intensities [11]. Specifically, we make the following observation: combined with a simple ensemble operation, **a masked pre-trained model can naturally denoise images with unseen noise degradation.**

Building upon the above observation, we introduce a zero-shot denoising paradigm, *i.e.*, Masked Pre-train then Iterative fill (MPI). Our pipeline starts with a model trained on ImageNet with pixel-wise masking strategy, which is further fine-tuned on a single image with unseen noise degradation. The pre-training phase provides more generic knowledge, which prevents premature over-fitting during denoising. Refinement phase is designed to predict masked regions, wherein only the predictions of these areas are preserved, thereby minimizing the gap between pre-training and fine-tuning. Moreover, rather than utilizing fixed weights post fine-tuning, we perform ensemble directly within fine-tuning iterations for efficiency, resulting in a fill-based iterative ensemble scheme, allowing us to achieve impressive results within 200 iterations. Benefiting from the effective cooperation of pre-training and fine-tuning, we are enabled to handle a wider range of noise scenarios with less information about noise patterns or intensities. Remarkably, we find that the extracted representation can even generalize to images distinctly different from natural ones [54], underscoring the potential of our method in practical application.

The main contributions of this paper are as follows:

- We introduce a novel zero-shot denoising paradigm, *i.e.*, Masked Pre-train then Iterative fill (MPI), which introduces self-supervised pre-training in this context for the first time, to effectively address denoising of unseen noise degradation types with a single noisy image.
- We develop a pre-training scheme with pixel-wise masks to capture general distribution knowledge of natural images. To effectively fuse the pre-trained representations into denoising, we propose an iterative filling process, in which predictions of iterations are sequentially assembled according to their masks for high-quality output.
- Extensive experiments demonstrate the superiority, efficiency and robustness of MPI in diverse noisy scenarios. In a nutshell, MPI achieves significant performance gains across various noise types within reduced inference time,

highlighting its potential for practical applications.

2. Related Works

2.1. Unsupervised Image Denoising

Compared to supervised denoising techniques [24, 49, 51, 52], unsupervised approaches focus on situations when paired data is unavailable. Methods in this category include: **Paired noisy-noisy images.** To learn consistent representations from varied noise observations of the same scene, methods include [22] training on mapping from two noisy observations from the same scene. Additional approaches utilize supplementary noise data and synthetic noise to generate noisy pairs, as seen in [34, 35, 37, 55], as well as [6] learns shared latent from multiple noise observations.

Unpaired noisy-clean images. Du *et al.* [12] proposed to learn decoupled representations of contents and noise from images. Lin *et al.* [25] further utilizes separated noise representations to guide noise synthesis, thereby enhancing the denoising process. While Wu *et al.* [45] utilize a distillation loss from both real and synthetic noisy images.

Noisy images only. Techniques like blind-spot [20, 43–45], substitution followed by image reconstruction [4, 19], multiple sub-sampled images from a single noisy scene [16] or above approaches combined [17, 21, 36] are developed when only one observation is available from a noise scene.

In the context of zero-shot denoising tasks, where only one noisy image is visible during training, making it more challenging compared to methods mentioned above.

2.2. Zero-shot Image Denoising

Compared to unsupervised methods, zero-shot denoising is more challenging as it aims to restore from unknown noisy degradation with a single noisy image available. Typical strategies involve utilizing spatial correlations [8, 28], variation based priors [7, 48] or low-frequency characteristics of images, corrupting and reconstructing part of images [4, 19, 39], or constructing paired training sets from sub-sampled noisy images [23, 30]. Among which Noise2Void [19] is initially designed for learning from multiple noisy images, shows promise in its zero-shot version. Noise2Self [4] masks the input image with cyclically varying masks and learns reconstruction. Although there is a gap compared to supervised or unsupervised methods. While dropout-ensemble [39] is adapted on a noisy image for better performance, it requires over-smoothing and incurs large computational costs. Noise2Fast [23] and Zero-Shot Noise2Noise [30] are fast but struggle to completely remove noise from images, resulting in suboptimal visual results. DIP [41] and its variants [9, 15] exploits the features of deep networks to learn mappings from random noise to images. Early stopping [40] or other approaches [2, 18] are used to prevent over-fitting, and FasterDIP [27] further

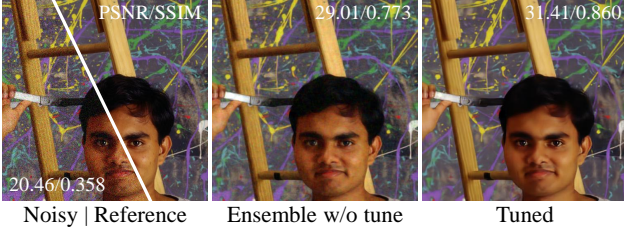


Figure 2. Motivation. A model trained on ImageNet with masking strategy, and ensembles with fixed parameter can denoise with averaging predicted results (“Ensemble w/o tune”), and its performance can be further improved with deliberately designed fine-tuning strategy (“Tuned”).

discusses the influence of network structure on its performance. However, current zero-shot methods often takes a long time, and parameter settings are carefully selected for various image contents and noise degradations.

2.3. Masked Image Modeling

Masked Image Modeling (MIM) helps in learning pre-trained representations for downstream tasks by masking a portion of input images [3, 14, 46] and training models to predict the masked contents. Due to its impressive effects in high-level tasks [31, 50], Masked Image Modeling has also found applications in low-level visual tasks. For instance, Wang *et al.* [42] applies random patch masks during the pre-training of image deraining and desnowing models in handling adverse weather conditions. Zheng *et al.* [56] integrates Masked Autoencoder (MAE) to learn illumination-related structural information in a supervised low-light enhancement framework. Notably, despite the successful applications of Masked Image Modeling in several low-level vision tasks, its application in the pre-training scheme for denoising models has not yet been explored.

3. Methods

In Sec. 3.1, we first investigate the properties of models trained with masking, proving that models trained with masking strategy can learn representations beneficial for denoising. Based on our observation, we deliberately design a zero-shot denoising paradigm that includes pre-training (see Sec. 3.2) and iterative fine-tuning (see Sec. 3.3).

3.1. Motivation

Masked Image Modeling [3, 14, 46] have achieved remarkable success in the field of computer vision. These models, trained on numerous images to capture distribution representations of natural images, suggesting potential applicability under diverse scenarios, have been proven beneficial for high-level downstream tasks [31, 50].

To further explore its capabilities in denoising, we train a model on vast natural images with pixel-level random masks (for details, see Sec. 3.2) and assess its performance

against a target image with unseen noise distribution. Surprisingly, we observe that a simple average of predictions from a fixed-state trained model achieves remarkably good denoising performance on unseen noise, and an example is presented in Fig. 2. This observation suggests that **a masked pre-trained model can serve as a natural image denoiser**. However, artifacts exist in the results, which can be attributed to the lack of knowledge about specific degradation patterns in the target image.

Drawing on the above observation, we design an efficient zero-shot denoising pipeline that enhances pre-trained knowledge by efficiently incorporating the noise distribution from a single noisy image, as shown in Fig. 3, *i.e.* Masked Pre-train then Iterative fill. First, a model is pre-trained with random mask M and corresponding element-wise negation \hat{M} to learn distribution knowledge related to natural images, which is formulated as:

$$\arg \max_{\theta} p(I \odot \hat{M} | I \odot M; \theta), \quad (1)$$

where I indicates natural image without any degradation priors, which is typically from large natural image datasets (*e.g.* ImageNet [11]). The operation \odot is element-wise multiplication. Then pre-trained network parameter θ is fine-tuned with noisy input x in t -th prediction, and predictions are assembled to achieve the final denoised image \bar{y} :

$$\bar{y} = Ensemble\{\mathcal{D}_{\theta_t}(x)\}_{t=1}^T, \quad (2)$$

where $\mathcal{D}_{\theta_t}(\cdot)$ is network parameterized by θ_t , fine-tuned from original θ . Masked Pre-training process is described in Sec. 3.2, while Ensemble process is described in Sec. 3.3.

3.2. Masked Pre-training

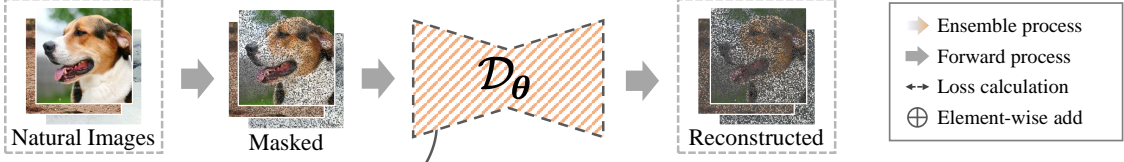
Masking strategy. Unlike the MAEs trained for high-level tasks, due to the difference in “semantics” required for low-level and high-level tasks [26], we implement a specialized masking strategy to achieve finer-grained image representations, *i.e.*, a pixel-wise masking strategy. Specifically, given an input image $I \in \mathbb{R}^{H \times W \times C}$ divided into random patches of size 1, a subset of them are randomly replaced by mask token with probability p (for further discussion about p , see Sec. 4.6 and Fig. 9). When the mask token is set to 0, the masked image $\hat{M} \odot I$ with random mask $M \in \mathbb{R}^{H \times W \times C}$ corresponds to a bernoulli sampling of the input image I . For each element $M_{[k]}$ in M , we have:

$$M_{[k]} = \begin{cases} 0, & \text{with prob. } p; \\ 1, & \text{with prob. } 1 - p. \end{cases} \quad (3)$$

Pre-training scheme. During pre-training, the network $\mathcal{D}_{\theta}(\cdot)$ is trained to learn recovering natural image I itself with random mask M :

$$\tilde{I} = \mathcal{D}_{\theta}(M \odot I). \quad (4)$$

1. Pre-training



2. Fine-tuning

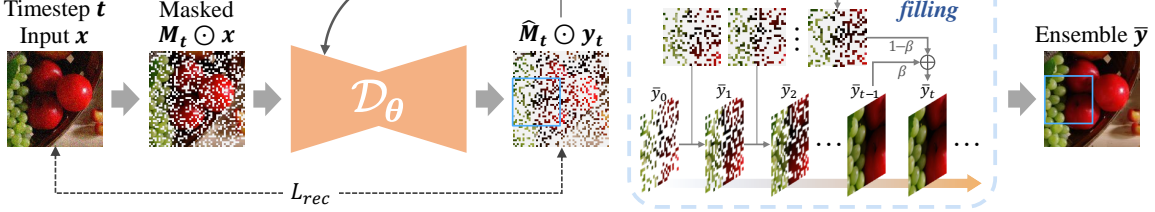


Figure 3. An overview of the proposed MPI paradigm that consists of Masked Pre-training and Iterative filling. During pre-training $\mathcal{D}_\theta(\cdot)$ learns to reconstruct from masked natural images. In the fine-tuning stage, with pre-trained representations θ and deliberately designed ensemble mechanism, we can inference corresponding clean image \bar{y} on an image with unknown noise degradation x .

We set the same optimization strategy outlined in [46], where the computation of the loss is restricted exclusively to the masked regions of prediction \tilde{I} , thus directing the network’s full attention toward the reconstruction of these areas, denoted as L_{rec} :

$$L_{rec}(\tilde{I}, I) = \left\| \hat{M} \odot \tilde{I} - \hat{M} \odot I \right\|_2. \quad (5)$$

The Mean Squared Error (MSE) loss is adopted to learn a relatively smoother representation.

For the architecture of network $\mathcal{D}(\cdot)$, we employ the same U-shaped hourglass architecture as in DIP [41], which has been proven a powerful zero-shot denoising architecture [27]. Furthermore, its relatively small network parameter configuration enables accelerated training, alleviating potential computational costs during fine-tuning and rendering it more appropriate for zero-shot denoising tasks.

3.3. Iterative Filling

Overall design. As observed in Sec. 3.1, an iterative fine-tuning process is carefully designed to address artifacts caused by input noise for improved performance. Unlike the common approach where MIMs [14, 46] are followed by supervised fine-tuning with full images as input, since our fine-tuning task does not have access to clean labels, we employ a self-supervised approach to learn the mapping from a noisy image to itself. However, this direct self-mapping approach would result in significant gap between the fine-tuning and pre-training tasks, making it challenging to achieve good performance in a short number of steps and with only a single noisy image visible.

Considering above challenges, we retain the same random masks applied in Sec. 3.2 for both the input and loss computation, leading to a pixel-based iterative refinement

process, in which only the predicted parts covered by random masks are assembled, for input noisy image x , random mask M_t and its element-wise negation \hat{M}_t in t -th iteration, prediction y_t and assembled result \bar{y} can be derived:

$$y_t = \mathcal{D}_{\theta_t}(M_t \odot x); \quad (6)$$

$$\bar{y} = \sum_t a_t \cdot y_t \odot \hat{M}_t, \quad (7)$$

where θ_t indicates the network parameter in each iteration, a_t is corresponding coefficients where $\sum_t a_t = 1$. The optimization objective at each iteration is as follows:

Algorithm 1: Iterative filling. Fine-tuning pipeline designed to leverage pre-trained representation θ for zero-shot denoising.

Input: Noisy image x , pre-trained parameter θ , network $\mathcal{D}(\cdot)$, exponential weight β , masking ratio p .

Output: denoised ensemble \bar{y} from predictions of iteration $\{y_t\}$.

load parameter θ for $\mathcal{D}(\cdot)$ as θ_1

initialize \bar{y}

for t from 1 to T **do**

 generate random mask M_t with mask ratio p

$y_t = \mathcal{D}_{\theta_t}(M_t \odot x)$

$\hat{M}_t = \neg M_t$

$\theta_{t+1} = \theta_t - \nabla_\theta \left\| \hat{M}_t \odot y_t - \hat{M}_t \odot x \right\|_2$

$\bar{y} \leftarrow \hat{M}_t \odot (\beta \cdot \bar{y} + (1 - \beta) \cdot y_t) + M_t \odot \bar{y}$

end

return \bar{y}

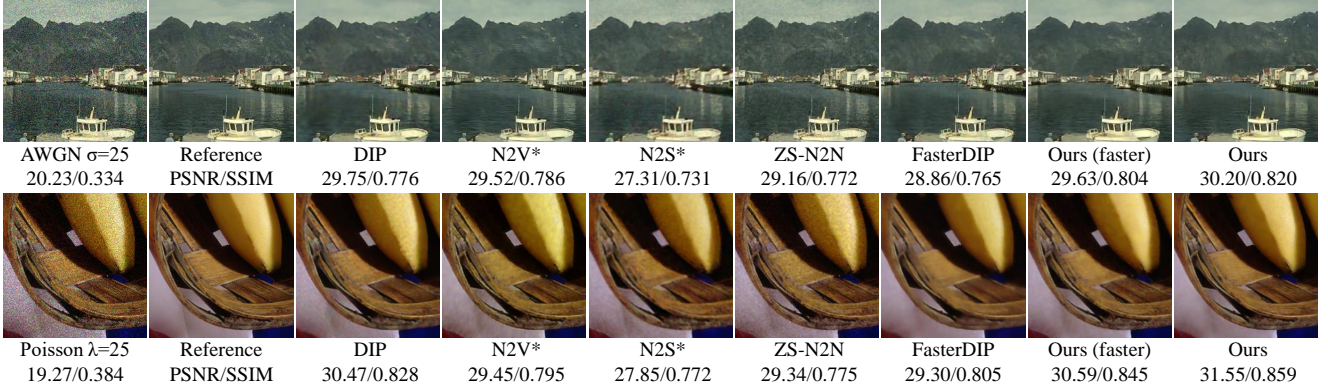


Figure 4. Qualitative denoising results on AWGN and Poisson noise. The quantitative PSNR/SSIM results are provided underneath. Noisy patches are from CBSD-44 and McMaster-14, respectively. Best viewed in color (zoom-in for a better comparison).

Table 1. Quantitative comparison of different methods on CSet, McMaster and CBSD dataset for AWGN removal ($\sigma \in [10, 25, 50]$). The best results are highlighted in **bold**, while the second best is underlined.

	σ	DIP [41]	N2V* [19]	N2S* [4]	ZS-N2N [30]	FasterDIP [27]	Ours (faster)	Ours
CSet [8]	10	32.05/0.829	31.55/0.885	28.04/0.819	<u>33.87/0.883</u>	31.59/0.815	<u>33.84/0.890</u>	34.95/0.910
	25	30.42/0.795	29.39/0.814	28.19/0.777	29.55/0.765	30.19/0.766	<u>30.83/0.824</u>	31.60/0.840
	50	24.73/0.533	27.35/0.694	26.62/0.699	26.10/0.624	26.09/0.669	<u>28.07/0.706</u>	28.15/0.704
McMaster [53]	10	32.48/0.878	30.98/0.877	28.61/0.839	34.19/0.908	31.48/0.842	<u>34.34/0.921</u>	35.50/0.937
	25	<u>31.07/0.856</u>	29.11/0.833	27.59/0.776	29.37/0.786	29.47/0.794	<u>30.99/0.863</u>	31.90/0.879
	50	25.72/0.639	24.65/0.676	24.89/0.673	25.82/0.634	24.75/0.663	<u>28.17/0.767</u>	28.31/0.758
CBSD [32]	10	31.18/0.865	31.18/0.918	28.17/0.853	33.73/0.923	30.89/0.857	<u>34.22/0.935</u>	35.16/0.947
	25	29.29/0.828	27.51/0.812	26.93/0.796	29.01/0.815	28.57/0.806	<u>30.01/0.854</u>	30.56/0.865
	50	23.06/0.540	<u>25.74/0.700</u>	24.78/0.695	25.37/0.657	24.75/0.669	<u>26.88/0.702</u>	26.71/0.700
Avg. Infer. time (s)		451.9	153.9	147.9	<u>22.2</u>	149.2	18.8	100.0

Table 2. Quantitative comparison of different methods on CSet, McMaster and CBSD dataset for Poisson noise removal (Average of $\lambda \in [10, 25, 50]$). See more details in supplementary material.

Methods	CSet [8]	McMaster [53]	CBSD [32]
DIP [41]	26.83/0.650	28.27/0.767	26.00/0.704
N2V* [19]	27.85/0.741	28.47/0.791	26.13/0.773
N2S* [4]	26.73/0.730	26.91/0.773	25.88/0.755
ZS-N2N [30]	27.85/0.703	28.31/0.766	27.49/0.757
FasterDIP [27]	27.20/0.697	27.62/0.768	26.03/0.727
Ours(faster)	<u>29.44/0.763</u>	<u>30.07/0.843</u>	<u>28.45/0.803</u>
Ours	29.69/0.766	30.51/0.842	28.62/0.810

$$\arg \min_{\theta_t} \left\| \hat{M}_t \odot y_t - \hat{M}_t \odot x \right\|_2. \quad (8)$$

The fine-tuning task, represented by $L_{rec}(y_t, x)$, is consistent with our pre-training task. The alignment not only minimizes the gap between pre-training and fine-tuning to avoid over-fitting but also reduces the number of fine-tuning iterations required, achieving desired denoising effect in a shorter period of time. Thanks to the well-crafted iterative filling and fine-tuning mechanisms, we manage to accomplish high-quality results with preserved details within reduced time **without any other regularization**.

Pixel-based iterative refinement. Ensemble methods have been proven beneficial for denoising tasks, as evidenced

by [18, 39]. To maximize the utilization of fine-tuned predictions in line with the optimization objectives of the fine-tuning task, we propose a pixel-based refinement approach, described in Eq. (7). For each iteration, only the regions indicated by \hat{M} are updated, while the remaining areas are left unchanged. The updates are conducted according to an Exponential Moving Average (EMA) strategy:

$$\bar{y} = \hat{M}_t \odot (\beta \cdot \bar{y} + (1 - \beta) \cdot y_t) + M_t \odot \bar{y}. \quad (9)$$

A more detailed description of proposed ensemble algorithm can be found in Alg. 1. During fine-tuning, the powerful pre-trained weights not only provide a better startup but also act as regularization for the network, preventing it from over-fitting too early and leading to better performance with less inference time (see Sec. 4.6).

Ensemble strategy. To utilize the predictions from each iteration with efficiency, we explore various ensemble strategies, including the above-mentioned EMA-based strategy, straightforward averaging strategy during iterations and average after fine-tuning. The straightforward averaging strategy during iterations is labeled as “**average**”. Average after fine-tuning, specifically, is to fix the model weights after a specific number of fine-tuning iterations, and then average the results from predictions as the final denoising output, noted as “**avg after 400/500/600e**”. Regardless of whether assembling all predictions during fine-tuning or after fine-



Figure 5. Qualitative denoising results on unseen noise types. Restormer is trained with AWGN $\sigma=25$. Noisy patches are from kodim07 and kodim12. Best viewed in color (zoom-in for a better comparison).

Table 3. Quantitative analysis of unseen noise on Kodak. All supervised and unsupervised methods are trained on AWGN with $\sigma=25$ and tested on 5 typical noise types for generalization evaluation. (AWGN $\sigma=25$ is provided for reference, with average from all 6 settings.)

Test Noise	Supervised		Unsupervised		Zero-shot			
	SwinIR [24]	Restormer [49]	Nb2Nb [16]	B2U [43]	DIP [41]	ZS-N2N [30]	Ours (faster)	Ours
AWGN $\sigma=25$	<u>32.89/0.895</u>	33.04/0.897	32.06/0.880	32.26/0.880	30.05/0.806	29.46/0.775	30.94/0.848	31.78/0.865
AWGN $\sigma \in [10, 50]$	27.29/0.628	30.00/0.729	28.68/0.713	29.24/0.726	29.56/0.783	29.36/0.753	<u>30.89/0.837</u>	31.66/0.846
Poisson $\lambda \in [10, 50]$	25.06/0.622	26.52/0.683	27.31/0.703	28.22/0.718	28.67/0.758	28.17/0.732	<u>29.94/0.826</u>	30.57/0.832
NLF from [38]	<u>32.52/0.862</u>	31.71/0.857	31.88/0.859	31.98/0.859	29.71/0.821	31.02/0.834	<u>32.26/0.886</u>	33.15/0.901
Speckle $v \in [10, 50]$	31.97/0.841	33.52/0.884	31.31/0.837	31.65/0.847	30.73/0.818	33.78/0.891	<u>34.79/0.924</u>	35.79/0.933
S&P $d \in [0.02, 0.05]$	23.96/0.614	23.63/0.613	27.04/0.686	29.44/0.796	29.54/0.800	<u>35.25/0.952</u>	<u>35.05/0.953</u>	36.87/0.964
Average	28.94/0.744	29.73/0.777	29.71/0.800	30.47/0.804	29.71/0.798	31.17/0.823	<u>32.31/0.879</u>	33.30/0.890

tuning, both result in reduced performance. Detailed comparison is shown in Sec. 4.6 and Table 6.

4. Experiments

We assess our method against several representative methods including DIP [41], Noise2Void (N2V) [19], Noise2Self (N2S) [4], Zero-Shot Noise2Noise (ZS-N2N) [30], and FasterDIP [27]. We modify the N2V and N2S to single-image version, name as N2V* and N2S*. The Peak Signal-to-Noise Ratio (PSNR) and Structure Similarity Index Measure (SSIM) are reported for comparison.

Evaluation is conducted under synthetic noise (Sec. 4.2 and Sec. 4.3) and real noise (Sec. 4.4). Furthermore, tests on medical images (Sec. 4.5) reveal that our pre-trained knowledge adapts well to images distinct from natural images. Ablation experiments are conducted in Sec. 4.6.

4.1. Experimental Setup

Pre-training. The pre-training process is based on two Nvidia RTX 3090 GPUs using Adam optimizer with $\beta_1 = 0.9$ and $\beta_2 = 0.9$. The initial learning rate is set as $2e^{-3}$ and decays to $1e^{-5}$ with cosine annealing strategy for 80K iterations with batch size set to 64. We initiate pre-training on randomly cropped 256×256 patches from subset of ImageNet [11] with 48,000 images. Within pre-training phase, a portion of image is masked with probability p , we apply $p = 0.3$ for synthetic noise, and higher ratio for spatial correlated noise. Further discussion of p is shown in Sec. 4.6.

Fine-tuning. For the pre-trained model, we set the learning rate during fine-tuning to $2e^{-3}$. We apply the same masking ratio p as pre-training. We set EMA weight $\beta = 0.99$ and ensemble for total 1000 iterations. In addition, with $\beta = 0.9$, we achieve performance surpassing most zero-shot methods within 200 iterations, denoted as “faster”.

4.2. AWGN & Poisson Noise

We investigate Additive White Gaussian Noise (AWGN) with noise levels $\sigma \in [10, 25, 50]$ and Poisson noise with $\lambda \in [10, 25, 50]$ separately on three popular datasets: CSet [8], McMaster [53] and CBSD [32], which consist of 9, 18 and 68 high-quality images, respectively. The results are shown in Table 1 and Table 2. The same experimental settings are applied to the model for different noise types, without prior knowledge of noise distribution or intensity.

Analysis. DIP tends to produce over-blurry results due to its frequency-based reliance, and struggles especially with intense noise. While ZS-N2N manages weak noise, its simple down-sample approach falters with stronger noise, thus causing artifacts. As Fig. 4 illustrates, under Gaussian noise $\sigma = 25$ and Poisson noise $\lambda = 25$, our method surpasses others in both noise reduction and detail preservation. In some cases, we see an improvement of over 1dB, highlighting the effectiveness of our proposed zero-shot paradigm.

As seen in Table 1, average inference time is listed. Our “faster” version achieve the fastest inference speed while surpassing comparing methods in most cases. Even our strategy with $\beta = 0.99$ exhibits competitive inference time

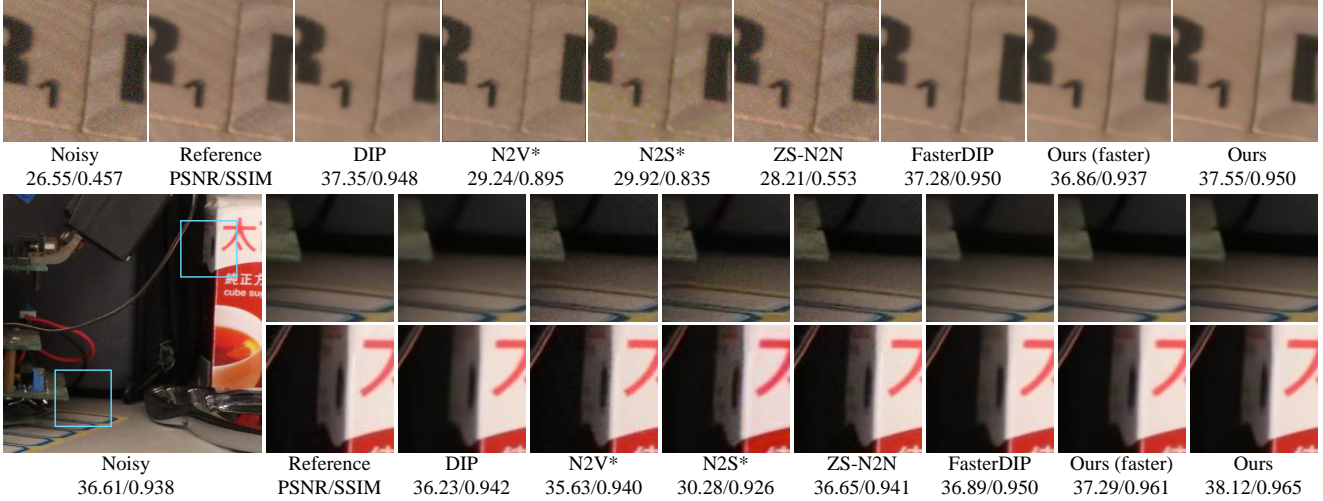


Figure 6. Qualitative denoising results on real noise removal from SIDD and PolyU. Noisy patches are from SIDDval31_1 and Canon80D.8.8.3200_ball.16. Zoom in for a better comparison.

Table 4. Quantitative comparison of different methods on SIDD, PolyU and FMD datasets for real noise removal.

Methods	SIDD [1]	PolyU [47]	FMD [54]
DIP [41]	33.66/0.800	37.91/0.952	32.85/0.840
N2V* [19]	26.42/0.546	32.82/0.930	31.61/0.759
N2S* [4]	26.63/0.531	35.04/0.921	29.79/0.817
ZS-N2N [30]	25.50/0.415	36.04/0.915	31.65/0.768
FasterDIP [27]	33.25/0.804	37.99/0.957	32.07/0.821
Ours (faster)	33.62/0.825	37.64/0.957	32.68/0.845
Ours	34.40/0.842	38.13/0.961	32.91/0.846

and significantly better performance. Details about Params and FLOPs are in supplementary materials.

4.3. Generalization on Unseen Noise

We believe that zero-shot denoising with knowledge from natural images offers new perspectives on improving the generalizability of denoising methods. We select several recent supervised methods (SwinIR [24], Restormer [49]) and unsupervised methods (Neighbor2Neighbor [16], Blind2Unblind [43]) for demonstration. These methods are trained on Gaussian noise with $\sigma = 25$ and tested on 5 unknown synthetic noise types on Kodak [13].

Analysis. As illustrated in Table 3 and Fig. 5, although methods trained on multiple noisy images achieve better results on noisy cases with the same distribution, they exhibit poor generalization performance. In contrast, zero-shot methods often perform better generalization capabilities, especially our method which achieves the best performance across all types of generalization noise.

4.4. Real Noisy Datasets

We validate the denoising capability of our method on synthetic noise in previous experiments. However, real-world noise is more complicated and challenging. We test

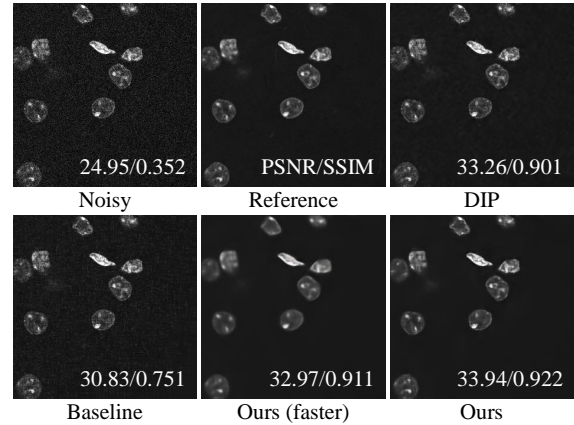


Figure 7. Validation of pre-trained representations on image differs from natural images. Comparing between “Baseline” (w/o pre-train) and “Ours” (w pre-train). Noisy patch is from TwoPhoton_MICE_3. See quantitative comparison at Table 5.

our method on SIDD [1] and PolyU [47] datasets, including 300 random patches from the SIDD validation and all 100 official patches from PolyU to prove our paradigm can benefit real images. Due to the significant differences between synthetic and real noise, all comparison methods are carefully adjusted to adapt to the spatially correlated noise.

Analysis. As shown in Table 4, our method excels over other zero-shot approaches on both datasets. This underlines our method’s effectiveness on real-world noise removal. Fig. 6 show our method’s capability to balance noise removal and detail retention. In essence, our method is adept at real-world denoising, offering a robust solution for image quality enhancement in challenging situations.

4.5. Generalization to Medical Images

The pre-trained model, has learned the feature distributions of natural images, raises a question: can this knowl-

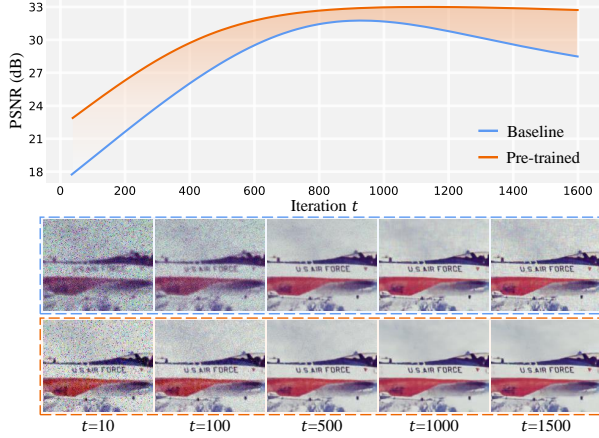


Figure 8. Effect of pre-trained model. Examples using AWGN $\sigma=25$ removal on F.16 with $\beta=0.99$. Pre-trained results are labeled in orange, while default initialized results are labeled in blue.

Table 5. Ablation of pre-trained weights, with defaults in gray .

β	Pretrain	CSet [8]	SIDD [1]	FMD [54]
0.99	✓	31.60/0.840	34.40/0.842	32.91/0.846
	✗	30.90/0.811	32.17/0.740	31.44/0.786
0.90	✓	30.83/0.824	33.62/0.825	32.68/0.845
	✗	30.10/0.806	33.23/0.819	32.31/0.833

edge be applied to other image types? To answer this question, we select a fluorescence microscopy dataset [54] characterized by colors and textures distinctly different from natural images. For comparison with other methods under the same settings as described in Sec. 4.4, see Table 4.

Analysis. We are surprised to find that the extracted knowledge from natural images still aids in denoising on the new dataset as well. As shown in “Baseline” and “Ours” in Fig. 7, the pre-trained knowledge prevents from overfitting to noise. In contrast, model without pre-training easily overfits to the noisy images, failing to successfully separate the noise from image. See quantitative comparison at Table 5.

4.6. Ablation Study

We discuss the effect of pre-trained weights, masking ratio and ensemble strategy in our proposed method, with most experiments conducted on CSet with $\sigma = 25$.

Pre-trained weights. Building upon the premise mentioned in Sec. 3.1, we question the role of pre-training in our paradigm by comparing model initialized with pre-trained weights to one with default initialized weights, which resembles a standard blind-spot approach. As shown in Fig. 8 and Table 5, due to the oversimplified task of content recovery from masked images, the latter quickly reaches its peak performance and begins to overfit, making it challenging to determine a specific iteration for all cases. Conversely, the pre-trained model improves steadily and maintains close-to-optimal performance for a more extended period.

Crucially, our approach introduces a new perspective.

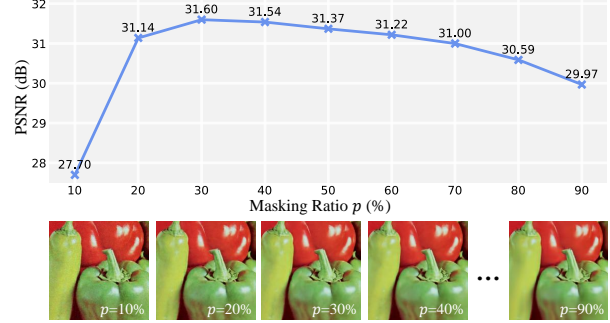


Figure 9. Effect of different mask ratios. Lower ratio lead to noisy result, while Higher ratio result in over-smoothed result. 30% is optimal for synthetic noise. Noisy patch is from Peppers.

Table 6. Ablation of ensemble strategy, default settings in gray .

Ensemble strategy	PSNR/SSIM	Infer. time (s)
Avg after 400e	30.87/0.793	95.1
Avg after 500e	30.88/0.793	109.3
Avg after 600e	30.84/0.792	120.9
Average	31.28/0.835	93.0
EMA w/o mask	23.48/0.441	100.2
EMA	31.60/0.840	101.4

Unlike other zero-shot techniques that start with a default initialized model to learn about noise-resistant image content, we’ve shown that a pre-trained model can aid in zero-shot tasks. The pre-trained weights, encapsulating views from multiple natural images, making it more robust to iteration count and thus achieving more robust performance.

Different masking ratios. Fig. 9 show the impact of different masking ratios on denoising. Paradigms with lower masking ratios fails to completely remove noise, while overly smoothed outcomes caused by higher masking ratios. For synthetic noise removal, a 30% masking ratio balances detail preservation and noise reduction. This contrasts with masking ratio $>70\%$ utilized in high-level tasks, highlighting different feature needs for task complexities.

Ensemble strategy. As mentioned in Sec. 3.3, we propose several ensemble strategy including “EMA”, “avg after 400/500/600e” and “average” with the same masking ratio for comparison, corresponding results are shown in Table 6. Proposed “EMA” achieve significant better performance, thus aiding denoising with efficiency.

Additionally, to validate our mask-based ensemble strategy, we remove the masks from Eq. (8) and Eq. (9), with full-pixel loss and ensemble, denoted as “EMA w/o Mask”. We observe a performance drop, as shown in Table 6, confirming the effectiveness of our proposed method.

5. Concluding Remarks

In this study, we introduce Masked Pre-train then Iterative fill (MPI), a zero-shot denoising paradigm utilizing pre-trained model with random masks to understand nat-

ural images. The extracted knowledge is fine-tuned through Iterative filling process, combining predictions with corresponding masks for enhanced quality and faster inference.

Broader impacts. From the perspective of our work, we have pioneered the use of generalizable knowledge from natural images without any assumptions about noise degradation, offering a unified framework for handling diverse synthetic and real noises. Notably, our zero-shot method excels in generalization compared to current supervised and unsupervised methods, offering new insights into denoising.

References

- [1] Abdelrahman Abdelhamed, Stephen Lin, and Michael S Brown. A high-quality denoising dataset for smartphone cameras. In *Proceedings of the IEEE conference on computer vision and pattern recognition*, pages 1692–1700, 2018. 7, 8
- [2] Metin Ersin Arican, Ozgur Kara, Gustav Bredell, andENDER Konukoglu. Isnas-dip: Image-specific neural architecture search for deep image prior. In *Proceedings of the IEEE/CVF Conference on Computer Vision and Pattern Recognition*, pages 1960–1968, 2022. 2
- [3] Hangbo Bao, Li Dong, Songhao Piao, and Furu Wei. Beit: Bert pre-training of image transformers. In *International Conference on Learning Representations*, 2021. 3
- [4] Joshua Batson and Loic Royer. Noise2self: Blind denoising by self-supervision. In *International Conference on Machine Learning*, pages 524–533. PMLR, 2019. 1, 2, 5, 6, 7
- [5] Haoyu Chen, Jinjin Gu, Yihao Liu, Salma Abdel Magid, Chao Dong, Qiong Wang, Hanspeter Pfister, and Lei Zhu. Masked image training for generalizable deep image denoising. In *Proceedings of the IEEE/CVF Conference on Computer Vision and Pattern Recognition*, pages 1692–1703, 2023. 1
- [6] Hao Chen, Chenyuan Qu, Yu Zhang, Chen Chen, and Jianbo Jiao. Multi-view self-supervised disentanglement for general image denoising. In *Proceedings of the IEEE/CVF International Conference on Computer Vision*, pages 12281–12291, 2023. 1, 2
- [7] Jun Cheng, Tao Liu, and Shan Tan. Score priors guided deep variational inference for unsupervised real-world single image denoising. In *Proceedings of the IEEE/CVF International Conference on Computer Vision*, pages 12937–12948, 2023. 1, 2
- [8] Kostadin Dabov, Alessandro Foi, Vladimir Katkovnik, and Karen Egiazarian. Image denoising by sparse 3-d transform-domain collaborative filtering. *IEEE Transactions on image processing*, 16(8):2080–2095, 2007. 1, 2, 5, 6, 8
- [9] Mohammad Zalbagi Darestani and Reinhard Heckel. Accelerated mri with un-trained neural networks. *IEEE Transactions on Computational Imaging*, 7:724–733, 2021. 2
- [10] Mauricio Delbracio and Peyman Milanfar. Inversion by direct iteration: An alternative to denoising diffusion for image restoration. *arXiv preprint arXiv:2303.11435*, 2023. 1
- [11] Jia Deng, Wei Dong, Richard Socher, Li-Jia Li, Kai Li, and Li Fei-Fei. Imagenet: A large-scale hierarchical image database. In *2009 IEEE conference on computer vision and pattern recognition*, pages 248–255. Ieee, 2009. 2, 3, 6
- [12] Wenchao Du, Hu Chen, and Hongyu Yang. Learning invariant representation for unsupervised image restoration. In *Proceedings of the IEEE/CVF conference on computer vision and pattern recognition*, pages 14483–14492, 2020. 1, 2
- [13] Rich Franzen. Kodak lossless true color image suite. *source: http://r0k.us/graphics/kodak*, 4(2):9, 1999. 7
- [14] Kaiming He, Xinlei Chen, Saining Xie, Yanghao Li, Piotr Dollár, and Ross Girshick. Masked autoencoders are scalable vision learners. In *Proceedings of the IEEE/CVF conference on computer vision and pattern recognition*, pages 16000–16009, 2022. 2, 3, 4
- [15] Reinhard Heckel and Paul Hand. Deep decoder: Concise image representations from untrained non-convolutional networks. In *International Conference on Learning Representations*, 2018. 1, 2
- [16] Tao Huang, Songjiang Li, Xu Jia, Huchuan Lu, and Jianzhuang Liu. Neighbor2neighbor: Self-supervised denoising from single noisy images. In *Proceedings of the IEEE/CVF conference on computer vision and pattern recognition*, pages 14781–14790, 2021. 1, 2, 6, 7
- [17] Yeong Il Jang, Keuntek Lee, Gu Yong Park, Seyun Kim, and Nam Ik Cho. Self-supervised image denoising with down-sampled invariance loss and conditional blind-spot network. In *Proceedings of the IEEE/CVF International Conference on Computer Vision (ICCV)*, pages 12196–12205, 2023. 2
- [18] Yeonsik Jo, Se Young Chun, and Jonghyun Choi. Rethinking deep image prior for denoising. In *Proceedings of the IEEE/CVF International Conference on Computer Vision*, pages 5087–5096, 2021. 1, 2, 5
- [19] Alexander Krull, Tim-Oliver Buchholz, and Florian Jug. Noise2void-learning denoising from single noisy images. In *Proceedings of the IEEE/CVF conference on computer vision and pattern recognition*, pages 2129–2137, 2019. 1, 2, 5, 6, 7
- [20] Samuli Laine, Tero Karras, Jaakko Lehtinen, and Timo Aila. High-quality self-supervised deep image denoising. *Advances in Neural Information Processing Systems*, 32, 2019. 2
- [21] Wooseok Lee, Sanghyun Son, and Kyoung Mu Lee. Apbsn: Self-supervised denoising for real-world images via asymmetric pd and blind-spot network. In *Proceedings of the IEEE/CVF Conference on Computer Vision and Pattern Recognition*, pages 17725–17734, 2022. 2
- [22] Jaakko Lehtinen, Jacob Munkberg, Jon Hasselgren, Samuli Laine, Tero Karras, Miika Aittala, and Timo Aila. Noise2noise: Learning image restoration without clean data. In *International Conference on Machine Learning*, pages 2965–2974. PMLR, 2018. 1, 2
- [23] Jason Lequyer, Reuben Philip, Amit Sharma, Wen-Hsin Hsu, and Laurence Pelletier. A fast blind zero-shot denoiser. *Nature Machine Intelligence*, 4(11):953–963, 2022. 1, 2
- [24] Jingyun Liang, Jie Zhang Cao, Guolei Sun, Kai Zhang, Luc Van Gool, and Radu Timofte. Swinir: Image restoration using swin transformer. In *Proceedings of the IEEE/CVF international conference on computer vision*, pages 1833–1844, 2021. 1, 2, 6, 7

- [25] Xin Lin, Chao Ren, Xiao Liu, Jie Huang, and Yinjie Lei. Unsupervised image denoising in real-world scenarios via self-collaboration parallel generative adversarial branches. In *Proceedings of the IEEE/CVF International Conference on Computer Vision*, pages 12642–12652, 2023. [2](#)
- [26] Yihao Liu, Anran Liu, Jinjin Gu, Zhipeng Zhang, Wenhao Wu, Yu Qiao, and Chao Dong. Discovering distinctive semantics in super-resolution networks. *arXiv preprint arXiv:2108.00406*, 2021. [3](#)
- [27] Yilin Liu, Jiang Li, Yunkui Pang, Dong Nie, and Pew-Thian Yap. The devil is in the upsampling: Architectural decisions made simpler for denoising with deep image prior. In *Proceedings of the IEEE/CVF International Conference on Computer Vision*, pages 12408–12417, 2023. [1](#), [2](#), [4](#), [5](#), [6](#), [7](#)
- [28] Matteo Maggioni, Vladimir Katkovnik, Karen Egiazarian, and Alessandro Foi. Nonlocal transform-domain filter for volumetric data denoising and reconstruction. *IEEE transactions on image processing*, 22(1):119–133, 2012. [1](#), [2](#)
- [29] Markku Makitalo and Alessandro Foi. Optimal inversion of the anscombe transformation in low-count poisson image denoising. *IEEE Transactions on Image Processing*, 20(1):99–109, 2011. [1](#)
- [30] Youssef Mansour and Reinhard Heckel. Zero-shot noise2noise: Efficient image denoising without any data. In *Proceedings of the IEEE/CVF Conference on Computer Vision and Pattern Recognition (CVPR)*, pages 14018–14027, 2023. [1](#), [2](#), [5](#), [6](#), [7](#)
- [31] Yunyao Mao, Jiajun Deng, Wengang Zhou, Yao Fang, Wanli Ouyang, and Houqiang Li. Masked motion predictors are strong 3d action representation learners. In *Proceedings of the IEEE/CVF International Conference on Computer Vision*, pages 10181–10191, 2023. [3](#)
- [32] David Martin, Charless Fowlkes, Doron Tal, and Jitendra Malik. A database of human segmented natural images and its application to evaluating segmentation algorithms and measuring ecological statistics. In *Proceedings Eighth IEEE International Conference on Computer Vision. ICCV 2001*, pages 416–423. IEEE, 2001. [5](#), [6](#)
- [33] Anish Mittal, Rajiv Soundararajan, and Alan C Bovik. Making a “completely blind” image quality analyzer. *IEEE Signal processing letters*, 20(3):209–212, 2012. [2](#)
- [34] Nick Moran, Dan Schmidt, Yu Zhong, and Patrick Coady. Noisier2noise: Learning to denoise from unpaired noisy data. In *Proceedings of the IEEE/CVF Conference on Computer Vision and Pattern Recognition*, pages 12064–12072, 2020. [2](#)
- [35] Reyhaneh Neshatavar, Mohsen Yavartanoo, Sanghyun Son, and Kyoung Mu Lee. Cvf-sid: Cyclic multi-variate function for self-supervised image denoising by disentangling noise from image. In *Proceedings of the IEEE/CVF Conference on Computer Vision and Pattern Recognition*, pages 17583–17591, 2022. [2](#)
- [36] Yizhong Pan, Xiao Liu, Xiangyu Liao, Yuanzhouhan Cao, and Chao Ren. Random sub-samples generation for self-supervised real image denoising. In *Proceedings of the IEEE/CVF International Conference on Computer Vision*, pages 12150–12159, 2023. [2](#)
- [37] Tongyao Pang, Huan Zheng, Yuhui Quan, and Hui Ji. Recorrupted-to-recorrupted: Unsupervised deep learning for image denoising. In *Proceedings of the IEEE/CVF conference on computer vision and pattern recognition*, pages 2043–2052, 2021. [2](#)
- [38] Tobias Plotz and Stefan Roth. Benchmarking denoising algorithms with real photographs. In *Proceedings of the IEEE conference on computer vision and pattern recognition*, pages 1586–1595, 2017. [6](#)
- [39] Yuhui Quan, Mingqin Chen, Tongyao Pang, and Hui Ji. Self2self with dropout: Learning self-supervised denoising from single image. In *Proceedings of the IEEE/CVF conference on computer vision and pattern recognition*, pages 1890–1898, 2020. [1](#), [2](#), [5](#)
- [40] Zenglin Shi, Pascal Mettes, Subhansu Maji, and Cees GM Snoek. On measuring and controlling the spectral bias of the deep image prior. *International Journal of Computer Vision*, 130(4):885–908, 2022. [1](#), [2](#)
- [41] Dmitry Ulyanov, Andrea Vedaldi, and Victor Lempitsky. Deep image prior. In *Proceedings of the IEEE Conference on Computer Vision and Pattern Recognition (CVPR)*, 2018. [1](#), [2](#), [4](#), [5](#), [6](#), [7](#)
- [42] Chao Wang, Zhedong Zheng, Ruijie Quan, Yifan Sun, and Yi Yang. Context-aware pretraining for efficient blind image decomposition. In *Proceedings of the IEEE/CVF Conference on Computer Vision and Pattern Recognition*, pages 18186–18195, 2023. [3](#)
- [43] Zejin Wang, Jiazheng Liu, Guoqing Li, and Hua Han. Blind2unblind: Self-supervised image denoising with visible blind spots. In *Proceedings of the IEEE/CVF Conference on Computer Vision and Pattern Recognition*, pages 2027–2036, 2022. [2](#), [6](#), [7](#)
- [44] Zichun Wang, Ying Fu, Ji Liu, and Yulun Zhang. Lg-bpn: Local and global blind-patch network for self-supervised real-world denoising. In *Proceedings of the IEEE/CVF Conference on Computer Vision and Pattern Recognition*, pages 18156–18165, 2023.
- [45] Xiaohe Wu, Ming Liu, Yue Cao, Dongwei Ren, and Wangmeng Zuo. Unpaired learning of deep image denoising. In *European conference on computer vision*, pages 352–368. Springer, 2020. [2](#)
- [46] Zhenda Xie, Zheng Zhang, Yue Cao, Yutong Lin, Jianmin Bao, Zhuliang Yao, Qi Dai, and Han Hu. Simmim: A simple framework for masked image modeling. In *Proceedings of the IEEE/CVF Conference on Computer Vision and Pattern Recognition*, pages 9653–9663, 2022. [2](#), [3](#), [4](#)
- [47] Jun Xu, Hui Li, Zhetong Liang, David Zhang, and Lei Zhang. Real-world noisy image denoising: A new benchmark. *arXiv preprint arXiv:1804.02603*, 2018. [7](#)
- [48] Zongsheng Yue, Hongwei Yong, Qian Zhao, Deyu Meng, and Lei Zhang. Variational denoising network: Toward blind noise modeling and removal. *Advances in neural information processing systems*, 32, 2019. [1](#), [2](#)
- [49] Syed Waqas Zamir, Aditya Arora, Salman Khan, Munawar Hayat, Fahad Shahbaz Khan, and Ming-Hsuan Yang. Restormer: Efficient transformer for high-resolution image restoration. In *Proceedings of the IEEE/CVF conference on*

computer vision and pattern recognition, pages 5728–5739, 2022. 2, 6, 7

- [50] Jiang-Tian Zhai, Xialei Liu, Andrew D Bagdanov, Ke Li, and Ming-Ming Cheng. Masked autoencoders are efficient class incremental learners. In *Proceedings of the IEEE/CVF International Conference on Computer Vision*, pages 19104–19113, 2023. 3
- [51] Kai Zhang, Wangmeng Zuo, Yunjin Chen, Deyu Meng, and Lei Zhang. Beyond a gaussian denoiser: Residual learning of deep CNN for image denoising. *IEEE Transactions on Image Processing*, 26(7):3142–3155, 2017. 1, 2
- [52] Kai Zhang, Wangmeng Zuo, and Lei Zhang. Ffdnet: Toward a fast and flexible solution for CNN based image denoising. *IEEE Transactions on Image Processing*, 2018. 1, 2
- [53] Lei Zhang, Xiaolin Wu, Antoni Buades, and Xin Li. Color demosaicking by local directional interpolation and nonlocal adaptive thresholding. *Journal of Electronic imaging*, 20(2): 023016–023016, 2011. 5, 6
- [54] Yide Zhang, Yinhao Zhu, Evan Nichols, Qingfei Wang, Siyuan Zhang, Cody Smith, and Scott Howard. A poisson-gaussian denoising dataset with real fluorescence microscopy images. In *Proceedings of the IEEE/CVF Conference on Computer Vision and Pattern Recognition*, pages 11710–11718, 2019. 2, 7, 8
- [55] Yi Zhang, Dasong Li, Ka Lung Law, Xiaogang Wang, Hongwei Qin, and Hongsheng Li. Idr: Self-supervised image denoising via iterative data refinement. In *Proceedings of the IEEE/CVF Conference on Computer Vision and Pattern Recognition*, pages 2098–2107, 2022. 2
- [56] Naishan Zheng, Man Zhou, Yanmeng Dong, Xiangyu Rui, Jie Huang, Chongyi Li, and Feng Zhao. Empowering low-light image enhancer through customized learnable priors. In *Proceedings of the IEEE/CVF International Conference on Computer Vision*, pages 12559–12569, 2023. 3